An electrochemical cell for *in operando* studies of lithium/sodium batteries using a conventional x-ray powder diffractometer

Yanbin Shen, Erik E. Pedersen, Mogens Christensen, and Bo B. Iversen[a)]
Center for Materials Crystallography, Department of Chemistry and iNANO, Aarhus University, Aarhus, Denmark

(Received 9 March 2014; accepted 2 September 2014; published online 10 October 2014)

An electrochemical cell has been designed for powder X-ray diffraction studies of lithium ion batteries (LIB) and sodium ion batteries (SIB) *in operando* with high time resolution using a conventional powder X-ray diffractometer. The cell allows for studies of both anode and cathode electrode materials in reflection mode. The cell design closely mimics that of standard battery testing coin cells and allows obtaining powder X-ray diffraction patterns under representative electrochemical conditions. In addition, the cell uses graphite as the X-ray window instead of beryllium, and it is easy to operate and maintain. Test examples on lithium insertion/extraction in two spinel-type LIB electrode materials ($Li_4Ti_5O_{12}$ anode and $LiMn_2O_4$ cathode) are presented as well as first results on sodium extraction from a layered SIB cathode material ($Na_{0.84}Fe_{0.56}Mn_{0.44}O_2$). © *2014 AIP Publishing LLC*. [http://dx.doi.org/10.1063/1.4896198]

I. INTRODUCTION

Lithium Ion Batteries (LIB) have achieved great success as portable power supply for consumer electronics in the last few decades, and it is now one of the most extensively studied energy storage devices.[1–4] Sodium Ion Batteries (SIB) are considered to have great potential in the application of renewable energy storage due to the abundance of sodium.[5–7] However, the decay of the electro-chemical performance of current batteries is still a main problem that limits their application in cases that require long cycle life and high safety. The performance reduction is mainly caused by the structural changes of the electrode materials inside the closed battery during charge/discharge. In addition, development of new electrode material with better performance (i.e., energy density, rate ability, and safety) to fulfill the growing requirements of the new applications also requires thorough understanding of the structural properties under working conditions of the battery. Hence, *in operando* monitoring of the structural evolution of battery materials is desirable, since this provides an in-depth understanding of the working mechanism and structural change of the electrode materials upon the LIB/SIB operation. Such studies are considered crucial for further development of battery technology.

Powder X-ray diffraction (PXRD) is a powerful tool for probing structural information in atomically ordered materials. It has been widely applied for structural studies of electrode material in LIB and SIB in the past few decades.[8–10] The development of *in situ* battery PXRD measurements provides a non-destructive and real-time understanding of critical structural processes occurring at the electrodes during the battery operation.[11–14] Measuring electrochemical properties and PXRD simultaneously enables observation of both the electronic and the structural transitions within the electrodes, providing insight into the complex reaction mechanisms and material stability of electrode materials under actual electrochemical processes. This makes it possible to optimize the performance of the material.

In operando PXRD investigations can be performed both on standard laboratory diffractometers and at synchrotron facilities.[12,14–17] Synchrotron sources provide X-ray beams with much higher photon flux compared with conventional X-ray tubes. However, the drawbacks are high cost, difficult and time limited access, complicated background due scattering from multiple components caused by the high penetrability of high energy X-rays, and possible peak overlaps due to the short wavelength of the X-rays. The insertion and extraction of Li/Na ion in electrode materials is a slow process, and in house conventional X-ray diffractometers provide much easier access to time consuming measurements since beam time at synchrotron sources is highly competitive. The recent development of high quality position sensitive detectors for the standard X-ray diffractometers that are common in many materials science laboratories also allows easier use of such techniques. The main problem for performing *in operando* PXRD studies with conventional powder diffractometers is the relatively lower photon flux. This means that the electrochemical cell must be carefully designed to minimize X-ray absorption during the measurement.

The electrochemical cell for *in operando* studies needs to be air tight to prevent exposure of the electrodes and electrolyte to water and air, and at the same time with a suitable window for X-ray transmission in order to get to the electrode material inside the closed system. The cell should also mimic real test cells and have a wide diffraction angle range. Finally, it should be convenient to assemble and disassemble in an inert glove box atmosphere. Most of the conventional electro-chemical cells for *in operando* PXRD studies are designed in a special shape that is quite different from the coin cells, and they may be fragile glass capillaries[18] or Swagelok-type design.[19,20] Such cells are primarily targeted for use at

a)Author to whom correspondence should be addressed. Electronic mail: bo@chem.au.dk

synchrotrons. Moreover, beryllium is usually used as X-ray window.[15,17,21,22] Beryllium is not only toxic, but will also dissolve in a liquid electrolyte when raised above 3 V, and hence an extra layer of conductive material is used for preventing the direct contact between the electrolyte saturated cathode and the beryllium window.[17,21] This makes the cell structure more complex and less user friendly in operation.

Here we present a novel design of an easily assembled electrochemical cell for *in operando* PXRD on a conventional laboratory X-ray diffractometer without the use of any beryllium components. This makes *in operando* studies easily accessible, cheap, and safe. The cell is very well sealed, operates in reflection mode, and allows fast data acquisition with good data quality. The key feature of the novel design is a very thin hemispherical graphite dome serving as the X-ray window and sealing component.

II. EXPERIMENTAL

A. Design of the electrochemical cell

Fig. 1 shows an overview of the electrochemical cell. It consists mainly of four parts. The first part is an aluminum cell base, which is used as a current collector for the electrode, and provides mounting on the diffractometer. The second part is a graphite dome (200 μm thick), which seals the cell, and also acts as X-ray window. It is sealed to the aluminum base with an O-ring using three screws. The third part is a lead knife-edge mounted on the aluminum base center blocking the diffracted beam coming of the graphite dome from the high intensity incoming X-ray beam. Finally, the fourth part is the main electrochemical cell components that are placed at the center of the aluminum base.

As shown in Fig. 2 in the arrangement of the electrochemical cell components, the bottom layer is a stainless steel (SS) holder, on top of which is placed the Li/Na foil anode electrode. The hole in the SS holder is to help centering the anode electrode and to give the thin electrode a clean and flat base. The cell separator, which is typically a polypropylene film or glass fiber, is placed on top of the Li/Na foil electrode. A polyoxymethylene gasket is placed around the disk holder to guide the separator and decrease the risk of direct contact between cathode and anode electrode. The Li/Na foil electrode and separator are wetted with electrolyte, which typically is a Li/Na salt, such as 1M $LiPF_6/NaClO_4$ dissolved in a mixture of carbonate solvents. The studied electrode is placed on top of the separator with the side consisting of active material facing the Li/Na anode, and the Al current collector side facing up. Finally, an Al plate with the design shown as in Fig. 2 is pressed on the Al current collector by four polyamide screws. Electronically insulated screw must be used here to prevent direct contact between cathode and anode. A thin stainless steel 16 mm ring with a 10 mm inner hole (not shown in Fig. 2) is mounted on the bottom side of the Al plate, to assure that only the stainless steel has contact with the electrolyte during the battery cycling. The Al current collector is directly in contact with this stainless steel ring and the contact area is about 98 mm^2 (56% of the total area). The top Al plate is designed with four special holes so that it can be easily pressed on the working electrode without applying strain on the electrode in the horizontal direction. The top Al plate is cut open in the center as a window for the X-rays to illuminate the working electrode. The electrode terminal of the working electrode is guided from the steel screw at the top Al plate and it gets out from the cell through a hole in the Al cell base, which is sealed with epoxy resin. The thin copper rod extending from the Al plate is the electrode terminal for the anode.

All of the cell components used here, including the Li/Na foil, the separator, the electrolyte, and the working electrode, are exactly the same as the ones used in a 2025 coin cell, which assures that the electrochemical performance data are comparable to standard coin cell data. With this arrangement, the working electrode is higher than the polyoxymethylene

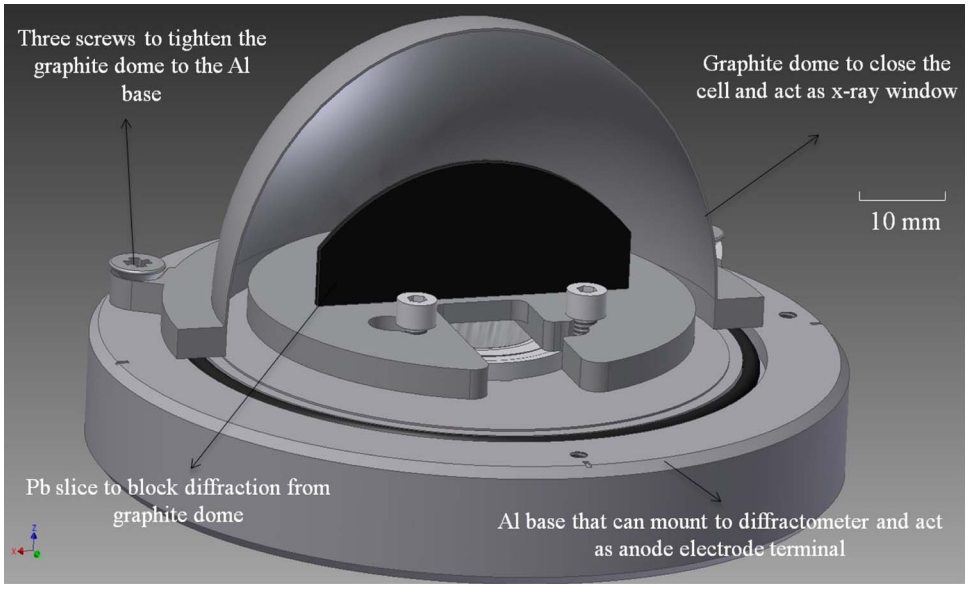

FIG. 1. Overview of the electrochemical cell.

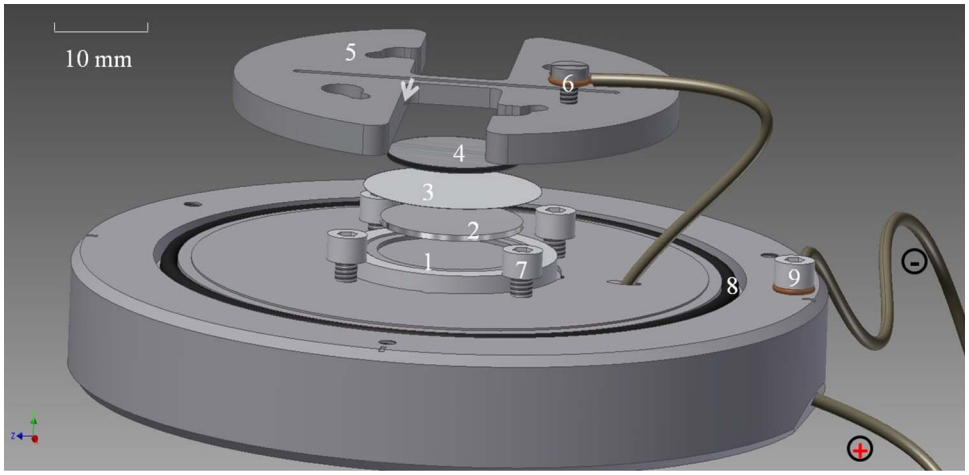

FIG. 2. Detailed arrangement of the electrochemical cell with the first type configuration: (1) Stainless steel holder with polyoxymethylene gasket, (2) lithium/sodium anode, (3) PE separator or glass fiber, (4) working electrode coated on the bottom side of a 15 μm thick Al foil, (5) Al/SS plate to press all the layers together and act as current collector (SS ring not shown), (6) working electrode terminal, (7) polyamides screws to tighten the Al plate and insulate the two electrodes, (8) O-ring for sealing, (9) anode electrode terminal.

gasket ensuring that data collection to low 2 theta values can be achieved. The gap between the Al plate and working electrode (indicated by the white arrow in Fig. 2) is big enough to ensure that data can also be collected at highest 2 theta angles. In this arrangement, the X-rays will always be transmitted through the Al current collector before diffraction occurs from the active material of the working electrode.

For lithium ion batteries, the cell components can also be arranged in an alternative configuration. The studied electrode can be placed on the SS holder, and this is the case where a Cu current collector is used. The Li anode is then on top of the separator and the X-rays penetrate the Li anode before scattering of the electrode. Generally, the working electrode is placed at the top, since we currently use a thick Li anode (0.6 mm) and a very thin Al current collector (15 μm) for the electrodes. The percentage of X-ray transmission for a wavelength of 1.54 Å through the various cell components is shown in Table S1 of the supplementary material.[23] All the data shown in this paper were collected with the first configuration as shown in Fig. 2.

B. *In operando* PXRD measurement

Two spinel type materials ($Li_4Ti_5O_{12}$ and $LiMn_2O_4$) and a layered type sodium cathode material ($Na_{0.84}Fe_{0.56}Mn_{0.44}O_2$) were selected to test the electrochemical cell. $Li_4Ti_5O_{12}$ is famous as a zero-strain anode material for both LIB and SIB.[24,25] $LiMn_2O_4$ is a cathode material which is non-toxic, low cost, and easy to prepare.[26,27] The spinel structure of both these materials offers a 3D diffusion pathway for Li/Na ion insertion/extraction, giving them high potential for applications in power tools and hybrid electric vehicles. The spinel materials were selected for demonstrating the performance of the *in situ* cell as they behave very differently upon lithium insertion/extraction even though their structures are similar. The $Li_4Ti_5O_{12}$ and $LiMn_2O_4$ particles were purchased from MTI Corporation. The third material discussed here is a layered type cathode material $Na_{0.84}Fe_{0.56}Mn_{0.44}O_2$ used for SIB. This material was prepared by a co-precipitation and solid state process using appropriate amounts of sodium carbonate, sodium oxalate, iron(III)nitrate nonahdyrate, and mangnaese(II)nitrate tetrahdyrate as initial reagents.

C. Battery assembly

All of the working electrode materials were prepared by thoroughly mixing 80 wt.% of active material, 10 wt.% acetylene black, and 10 wt.% polyvinylidene difluoride (PVdF) binder in N-methyl-2-pyrrolidone (NMP). The obtained electrode mixture was coated onto an aluminum foil with a coating bar and dried overnight under pre-vacuum at 100 °C. The electrodes were punched in the shapes of 12 mm diameter disks. For the LIB cells, metallic lithium foil was used as anode, and the cathode and anode were separated by two polypropylene membranes wetted in a commercially available standard electrolyte (1M $LiPF_6$ in ethylene carbonate (EC) : dimethyl carbonate (DMC) : diethyl carbonate (DEC) 4:3:3 in volume; MTI corporation). For the SIB cell, metallic sodium foil was used as anode. The used electrolyte was 1M $NaClO_4$ mixed with propylene carbonate (PC) with 2 vol.% of fluorinated ethylene carbonate (FEC) as additive. The separator was porous glass fiber (Whatman, GF/D). The electrochemical cell was assembled in an Ar filled glove box as described above. An argon atmosphere was maintained in the cell by sealing the cell using the graphite dome.

D. Measurements

Cycling of the cell during *in operando* PXRD measurements was performed using an MTI battery analyzer. Two $Li/LiMn_2O_4$ cells were cycled in the range of 2.75–4.30 V at, respectively, ∼0.08 C and 0.17 C rate (1 C rate indicate discharge of all the capacity in 1 h) in a constant current (CC) mode. The $Li/Li_4Ti_5O_{12}$ cell was discharged/charged between 1.0 V and 3.0 V at ∼0.08 C in a CC mode. The

$Na/Na_{0.84}Fe_{0.56}Mn_{0.44}O_2$ cell was tested in a similar way as the $LiMn_2O_4$ cell in the voltage range between 2.0 V and 4.0 V. The XRD patterns were collected in a parallel beam geometry using a Rigaku Smartlab diffractometer equipped with a rotating anode CuK_α radiation source and a D-tex/Ultra solid state detector. The rotating anode generator was operated at 40 kV, 180 mA, and the XRD patterns were measured in steps of 0.015° over the 2θ range of 35°–65° (15°–65° in the $Na_{0.84}Fe_{0.56}Mn_{0.44}O_2$ case). The height alignment was done based on the Bragg peak of the Al foil at $2\theta = 65.09°$. Each XRD pattern took ~18 min to measure, and Rietveld refinements were carried out using the Fullprof program.[28]

III. EXAMPLES OF MEASUREMENTS

A. $LiMn_2O_4$

The black curve (a) in Fig. 3 shows a typical XRD pattern of a fresh assembled $Li/LiMn_2O_4$ electrochemical cell prior to charging and discharging. It shows Bragg peaks from the cubic spinel cathode material and peaks of Al/Al_2O_3 from the Al current collector, which is a typical cathode current collector material. The latter also served as an internal standard in this study. As shown in the red curve (b) in Fig. 3, the Li anode peaks appear already when the loading of the electrode is 4.5 mg/cm^2 or lower. The loading of our electrode is usually ~5 mg/cm^2, which represents a sufficient thickness to avoid significant penetration into the layers below, and assuring that the probed volume is approximately kept constant. Compared with patterns obtained from electrochemical cells that use beryllium x-ray windows[17] or cells used at synchrotron sources in a transmission mode,[19] these XRD pattern shows well separated Bragg peaks, and they are largely free from strong background peaks. This leaves ample space for observing of the evolutions of the peaks from the active material. Due to the texture of the rolled Al and Li/Na foil, the diffraction patterns for these components have a strong dependence on orientation. The orientation dependence of Al and Li/Na has been reduced by rotating the electrode in the electrochemical cell (see the supplementary material[23]).

The contour plot in Fig. 4 shows a typical example of lithium ion extraction and insertion in the $LiMn_2O_4$ particles during the first charge/discharge cycle and a second charging between 4.3 V and 2.75 V at a constant current 0.08 C.

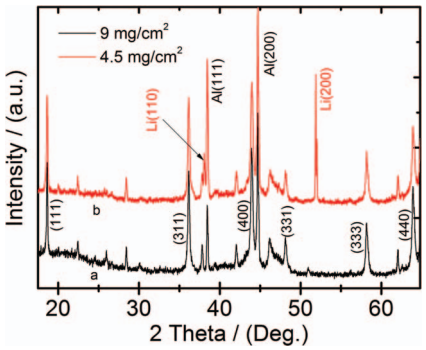

FIG. 3. XRD patterns from a freshly assembled $Li/LiMn_2O_4$ electrochemical cell with two different electrode loadings.

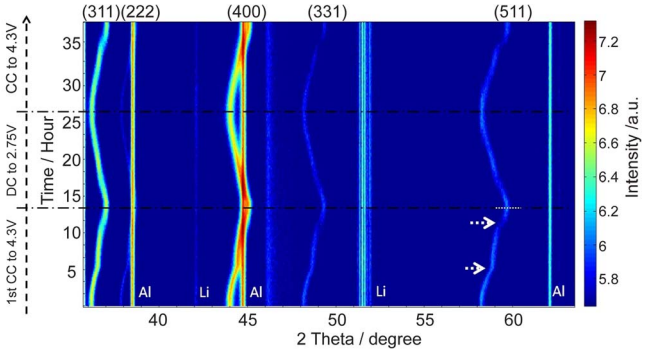

FIG. 4. Contour plot of XRD patterns from the $Li/LiMn_2O_4$ cell at the first charge/discharge cycle as well as the second charging at 0.08 C.

The corresponding plot for 0.17 C is shown in Fig. 5. Each PXRD pattern took ~10 min to measure. All the reflections having regular shifts during the charge/discharge cycle can be indexed to the spinel $LiMn_2O_4$ structure with space group Fd-3m. Additional strong reflections, which stay at constant 2θ positions, are from Al in the cathode current collector and from Li in the anode.

As the cell is charged, lithium ions are removed from the $LiMn_2O_4$ structure, and all the Bragg peaks shift to higher 2θ angles, indicating a contraction of the unit cell upon Li removal. When the cell was subsequently discharged and lithium ions reversibly intercalated back into the $LiMn_2O_4$ structure, all the Bragg peaks shifted to lower 2θ angles, implying a relaxation of the unit cell upon Li re-insertion. During the second charging of the cell, lithium ions were again extracted from the $LiMn_2O_4$ structure, and the Braggs peaks showed similar behavior as during the first charging. The symmetric change of the diffraction patterns indicates good reversibility of the electrochemical reaction in the electrochemical cell.

The shift of the Bragg peak positions is not linear. As indicated by the two arrows at the (511) peak, two sudden changes occur during the first charging of the battery. These sudden changes divide the PXRD patterns into three regions, suggesting that different cubic spinel phases are sequentially formed during the Li removal. This three-region

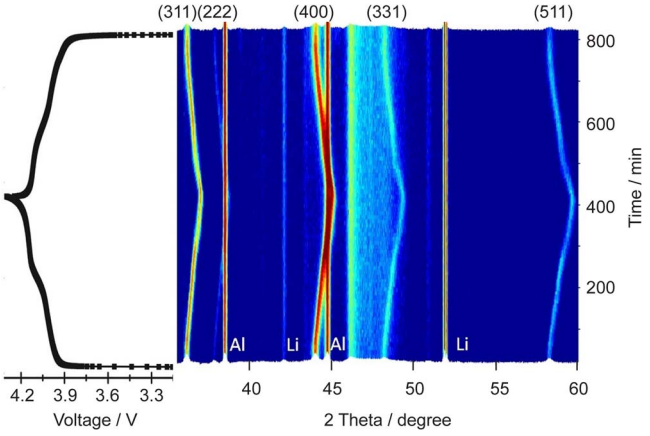

FIG. 5. Voltage profile (left) and contour plot of XRD patterns (right) of the first cycle of the $Li/LiMn_2O_4$ half cell charge/discharge at 0.17 C.

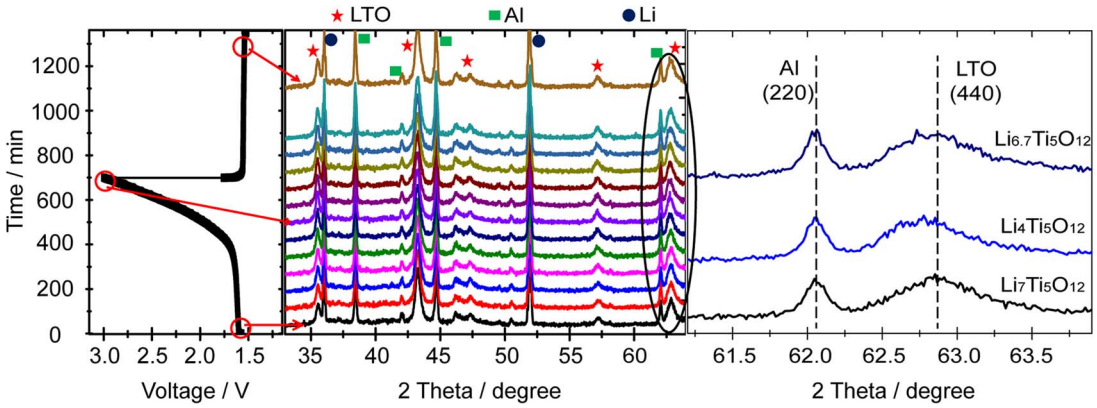

FIG. 6. Charge/discharge curve and the corresponding XRD patterns of the Li/$Li_4Ti_5O_{12}$ cell.

behavior agrees well with results reported in literature,[29] and it provides evidence that three distinct phases with spinel-type structure exist for the $Li_xMn_2O_4$ system. The phase separation could be due to reordering of atoms in the crystal structure at a certain level of Li removal. The evolution of the PXRD peaks (see the supplementary material[23]) is similar to what has been observed in other studies.[30]

When doubling the charge/discharge current (0.17 C), the trends in the PXRD peak shifts as well as the degree of change were the same, but the evolution shows less details (Fig. 5). This demonstrates the importance of developing electrochemical cells for *operando* studies using laboratory X-rays, where it is easier to conduct slow charge/discharge experiments. The charge/discharge profile of the Li/$LiMn_2O_4$ cell shows a typical three-region behavior as also observed in other studies using coin cells[31,32] confirming that the as-designed electrochemical cell provides reliable electrochemical data. Rietveld refinement results (see the supplementary material[23]) show that the unit cell dimension is reduced from 8.23787(3) Å to 8.05838(2) Å upon complete removal of Li, resulting in a ~2.18% contraction of the unit cell volume at the end of the first charge.

B. $Li_4Ti_5O_{12}$

The spinel $Li_4Ti_5O_{12}$ structure behaves very differently from the three-region behavior of the spinel $LiMn_2O_4$ structure observed in the PXRD patterns and the charge/discharge profile. As shown in Fig. 6, the spinel $Li_4Ti_5O_{12}$ structure has a very flat voltage curve at around 1.55 V, and the Bragg peaks have almost no change in position during the Li insertion/extraction. This indicates that the spinel $Li_4Ti_5O_{12}$ structure is much more stable upon Li insertion/extraction, and the results directly demonstrate the well known zero-strain property of this material. For clarity, only 13 PXRD patterns, which were recorded at equally spaced time intervals, are shown in Fig. 6. The red arrows pointing from the electrochemical voltage versus time plot to the PXRD scans indicate when the scans were collected. The 440 reflection is enlarged at the right side of Fig. 6, and it can be seen that it is slightly shifted to lower 2θ angle during charging from 1.6 V to 3.0 V. Then it reversibly returns to its original position during discharge to 1.5 V. This means that Li^+ insertion actually results in a lattice contraction, which is very different from the behavior of the spinel $LiMn_2O_4$. This might be attributed to the change of the Li^+ position from the 8a sites to the 16c sites in the lattice.

C. $Na_{0.84}Fe_{0.56}Mn_{0.44}O_2$

Unlike the spinel structure materials, which have cubic unit cells, and where the crystal structure change is equal in all the three direction during Li insertion/extraction, the O3-type layered $Na_{0.84}Fe_{0.56}Mn_{0.44}O_2$ material has a hexagonal unit cell with quite different unit cell changes during charge/discharge. The contour plot during the first charging is shown in Fig. 7(a), and the Bragg peaks belonging to the $Na_{0.84}Fe_{0.56}Mn_{0.44}O_2$ phase were selected (indicated in the red boxes) and shown in Fig. 7(b). The (003) and (006) Bragg peaks shift to lower 2θ angle upon the Na extraction indicating an expansion of the unit cell in the *c* direction. Simultaneously, the (110) peak shifts to higher 2θ angle, implying a contraction of the unit cell in the *a*- and *b*-directions. All the

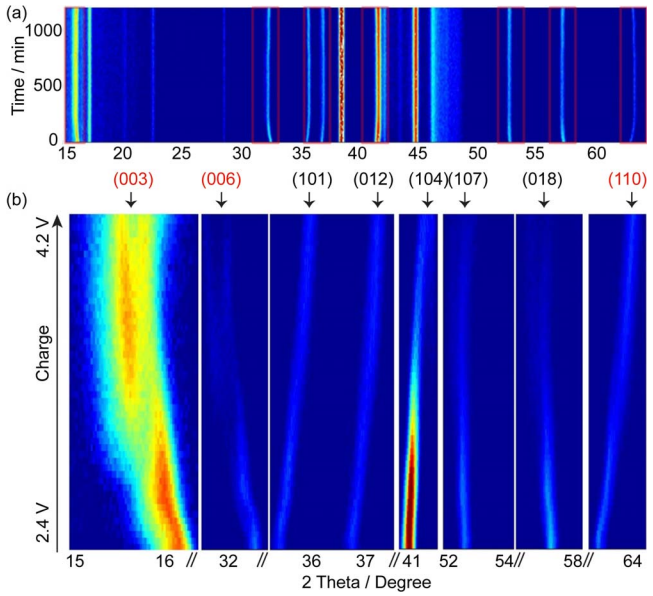

FIG. 7. (a) and (b) Contour plot of XRD patterns from the Na/$Na_{0.84}Fe_{0.56}Mn_{0.44}O_2$ cell during the first charge.

other Bragg peaks shown in Fig. 7 either expand or contract depending on the relative contributions from *a*, *b*, or *c*. At higher voltage with more Na insertion a phase transition occurred. This is evidenced by the new peak emerging at lower 2θ angle of the evanescent (003) peak. A more detailed study of this material will be reported elsewhere.

IV. CONCLUSIONS

We have designed a user friendly electrochemical cell for fundamental *in operando* structural investigations of electrode material of LIB/SIB using an in-house conventional powder X-ray diffractometer. The cell is free of beryllium X-ray windows, and mimics real test coin cells. It is easy to assemble without any special equipment. Approximately 110 XRD patterns were obtained per cycle when changing/discharging the battery at 0.08 C. The test results on the spinel type Li/$LiMn_2O_4$ cell show that the as-designed electrochemical cell is highly successful for structural evolution identification *in operando*. The diffraction patterns of the $Li_4Ti_5O_{12}$ anode upon Li insertion/extraction verified the almost zero-strain nature of this material. Finally, results from the layered SIB electrode material $Na_{0.84}Fe_{0.56}Mn_{0.44}O_2$ on the first charging showed very anisotropic crystal structure changes upon Na extraction, which is different from the isotropic changes observed in the spinel structure.

ACKNOWLEDGMENTS

The authors would like to thank the Danish National Research Foundation (DNRF93) for funding.

[1]V. Etacheri, R. Marom, R. Elazari, G. Salitra, and D. Aurbach, Energy Environ. Sci. **4**(9), 3243–3262 (2011).
[2]A. Yoshino, Angew. Chem. Int. Ed. **51**(24), 5798–5800 (2012).
[3]J. B. Goodenough and K.-S. Park, J. Am. Chem. Soc. **135**(4), 1167–1176 (2013).
[4]B. Scrosati and J. Garche, J. Power Sources **195**(9), 2419–2430 (2010).
[5]V. Palomares, P. Serras, I. Villaluenga, K. B. Hueso, J. Carretero-Gonzalez, and T. Rojo, Energy Environ. Sci. **5**(3), 5884–5901 (2012).
[6]M. D. Slater, D. Kim, E. Lee, and C. S. Johnson, Adv. Funct. Mater. **23**(8), 947–958 (2013).
[7]B. L. Ellis and L. F. Nazar, Curr. Opin. Solid State Mater. Sci. **16**(4), 168–177 (2012).
[8]J. R. Dahn and R. R. Haering, Solid State Commun. **40**(3), 245–248 (1981).
[9]J. Xie, X. Zhao, G. Cao, Y. Zhong, and M. Zhao, J. Electroanal. Chem. **542**(0), 1–6 (2003).
[10]H. M. Wu, J. P. Tu, Y. F. Yuan, Y. Li, X. B. Zhao, and G. S. Cao, Electrochim. Acta **50**(20), 4104–4108 (2005).
[11]J. N. Reimers and J. R. Dahn, J. Electrochem. Soc. **139**(8), 2091–2097 (1992).
[12]M. Balasubramanian, X. Sun, X. Q. Yang, and J. McBreen, J. Power Sources **92**(1–2), 1–8 (2001).
[13]G. G. Amatucci, J. M. Tarascon, and L. C. Klein, J. Electrochem. Soc. **143**(3), 1114–1123 (1996).
[14]M. Morcrette, Y. Chabre, G. Vaughan, G. Amatucci, J. B. Leriche, S. Patoux, C. Masquelier, and J. M. Tarascon, Electrochim. Acta **47**(19), 3137–3149 (2002).
[15]J. B. Leriche, S. Hamelet, J. Shu, M. Morcrette, C. Masquelier, G. Ouvrard, M. Zerrouki, P. Soudan, S. Belin, E. Elkaïm, and F. Baudelet, J. Electrochem. Soc. **157**(5), A606–A610 (2010).
[16]D. Mikhailova, A. Thomas, S. Oswald, W. Gruner, N. N. Bramnik, A. A. Tsirlin, D. M. Trots, A. Senyshyn, J. Eckert, and H. Ehrenberg, J. Electrochem. Soc. **160**(5), A3082–A3089 (2013).
[17]G. A. Roberts and K. D. Stewart, Rev. Sci. Instrum. **75**(5), 1251–1254 (2004).
[18]R. E. Johnsen and P. Norby, J. Appl. Crystallogr. **46**(6), 1537–1543 (2013).
[19]T. Gross, T. Buhrmester, K. G. Bramnik, N. N. Bramnik, K. Nikolowski, C. Baehtz, H. Ehrenberg, and H. Fuess, Solid State Ionics **176**(13–14), 1193–1199 (2005).
[20]C. Baehtz, T. Buhrmester, N. N. Bramnik, K. Nikolowski, and H. Ehrenberg, Solid State Ionics **176**(17–18), 1647–1652 (2005).
[21]M. N. Richard, I. Koetschau, and J. R. Dahn, J. Electrochem. Soc. **144**(2), 554–557 (1997).
[22]M. Morcrette, J.-B. Leriche, S. Patoux, C. Wurm, and C. Masquelier, Electrochem. Solid-State Lett. **6**(5), A80–A84 (2003).
[23]See supplementary material at http://dx.doi.org/10.1063/1.4896198 for computation of X-ray absorption.
[24]T. Ohzuku, A. Ueda, and N. Yamamoto, J. Electrochem. Soc. **142**(5), 1431–1435 (1995).
[25]L. Aldon, P. Kubiak, M. Womes, J. C. Jumas, J. Olivier-Fourcade, J. L. Tirado, J. I. Corredor, and C. Pérez Vicente, Chem. Mater. **16**(26), 5721–5725 (2004).
[26]J.-Y. Luo, Y.-G. Wang, H.-M. Xiong, and Y.-Y. Xia, Chem. Mater. **19**(19), 4791–4795 (2007).
[27]W. Tang, Y. Hou, F. Wang, L. Liu, Y. Wu, and K. Zhu, Nano Lett. **13**(5), 2036–2040 (2013).
[28]See https://www.ill.eu/sites/fullprof/ for FullProf.
[29]W. Liu, K. Kowal, and G. C. Farrington, J. Electrochem. Soc. **145**(2), 459–465 (1998)..
[30]T. Eriksson, A.-K. Hjelm, G. Lindbergh, and T. Gustafsson, J. Electrochem. Soc. **149**(9), A1164–A1170 (2002).
[31]S.-H. Kang, J. B. Goodenough, and L. K. Rabenberg, Chem. Mater. **13**(5), 1758–1764 (2001).
[32]A. Iqbal, Y. Iqbal, L. Chang, S. Ahmed, Z. Tang, and Y. Gao, J. Nanopart. Res. **14**(10), 1–14 (2012).